Edited by H. Ryssel, P. Pichler - September 1995

Fast and Accurate Aerial Imaging Simulation for Layout Printability Optimization

V. Axelrad

Technology Modeling Associates,
Palo Alto, CA, USA

1 Introduction

Optical lithography has been a major force in the continuing reduction of feature size in VLSI. Pushing the limits of lithography by using advanced lenses (high NA, in-lens filtering, etc.), light sources (annular, etc.) and mask designs (phase shift masks, optical proximity corrections, etc.) allowed to extend its life span far beyond what was predicted only 10 years ago.

Since lithographic image quality is a major limiting factor in VLSI processing, exact understanding of the printability of a certain layout is crucial to detect possible product quality problems. In certain cases it is possible to improve the image quality by optimizing the mask to compensate for non-local optical interaction effects (so-called optical proximity correction [1]). The ability to rapidly and accurately evaluate the expected image quality has therefore attained the status of considerable practical significance for industrial applications.

This work discusses the application of highly efficient algorithms based on the Fast Fourier Transform to achieve aerial image calculations many orders of magnitude faster than conventional lithography simulators such as DEPICT [2] and SPLAT [3]. An algorithm is presented which compares the original mask image with the calculated aerial image to estimate printability. The algorithm has essentially linear dependence of CPU time on image size and linear dependence of memory on image size, therefore full-chip applications are feasible. The current implementation requires approximately 1KB/μm^2 of memory and 40 ms/μm^2 CPU time on a SPARC Station 10. For a 500μm by 500μm image this translates into 250MB and 3 hours. Utilization of redundancy in regular layouts and windowing techniques can substantially reduce the requirements.

The techniques described here have been previously developed in connection with closely related wave propagation problems in acoustics [4], [5]. Applications of related techniques in lithography have also been reported [6].

2 The Method

Monochromatic wave propagation is governed by the well-known Helmholtz equation as well as appropriate boundary conditions:

$$\Delta\varphi + k^2\varphi = 0, \text{ with } k = \omega/c = 2\pi/\lambda \tag{1}$$

A general solution to this equation can constructed as an integral over all plane waves with the same wavelength $1/\lambda$ and amplitudes $\Phi(k_x, k_y)$ traveling in all directions given by the wave vector $\vec{k} = (k_x, k_y, k_z)$:

$$\varphi(x, y, z) = \int\int \Phi(k_x, k_y) \cdot e^{i(k_x x + k_y y + k_z z)} \cdot dk_x \cdot dk_y \tag{2}$$

Since the length of the wave vector k is given by equation (1), its z-direction component is the projection of the k-vector upon the z-axis:

$$k_z = \pm\sqrt{k^2 - (k_x^2 + k_y^2)} \qquad (3)$$

It is interesting to note that real values of k_z are only possible for $k_x^2 + k_y^2 \le k^2$. This means that only spectral components up to a certain cut-off frequency given by the wavelength are propagated, higher-frequency components are represented by so-called evanescent modes with imaginary k_z and are not present in the far field [4]. These modes are usually quite important in acoustics but of no significance in optics, where typical propagation distances through lenses are very much larger than the wavelength of light.

A physical interpretation of the Ansatz in eq. (2) is shown in Figure 1.: as the length of the projection of k onto the x-y plane approaches the total length of the k-vector given by the wavelength λ, its projection upon the z-axis decreases until it reaches zero. At this point the plane wave is traveling in the x-direction, orthogonally to the optical axis z. Beyond this point, higher values of $\sqrt{k_x^2 + k_y^2}$ do not correspond to real values of k_z:

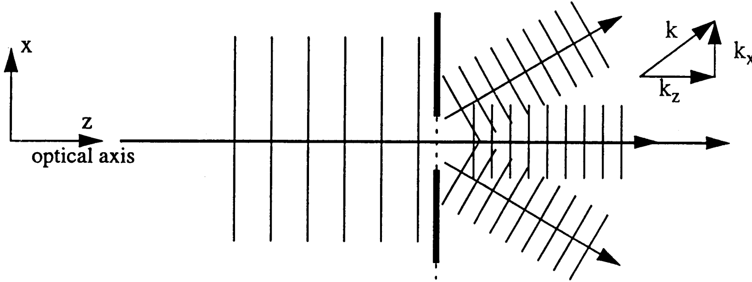

Figure 1. Physical interpretation of the Fourier Integral approach.

A two-dimensional inverse Fourier transform is recognized at the core of equation (2). We can therefore write the Fourier transform of the field in a plane z as a combination of forward and backward propagating waves for the two signs in equation (2):

$$\Phi(k_x, k_y; z) = \Phi^{forward}(k_x, k_y) \cdot e^{ik_z z} + \Phi^{back}(k_x, k_y) \cdot e^{-ik_z z} \qquad (4)$$

The aerial imaging problem as well as certain problems in acoustics are described by the special case of forward propagation only, i.e. reflections are not taken into account. For this case we skip the superscript *forward* and obtain the solution as:

$$\Phi(k_x, k_y; z) = \Phi(k_x, k_y; z_0) \cdot e^{ik_z(z - z_0)} \qquad (5)$$

Equation (5) is of central importance to the algorithm. It means that the Fourier transform of the field in the plane z can be calculated by multiplying the Fourier transform of the field in another plane z_0 by a linear space-invariant transfer function. In lithography, this transfer function can be used to model defocus, since a defocused image can be constructed as a propagation problem from the focus plane.

$$G(k_x, k_y; z - z_0) = e^{i\sqrt{k^2 - (k_x^2 + k_y^2)} \cdot (z - z_0)} \qquad (6)$$

Lens effects are taken into account by another transfer function. A perfectly focused ideal lens creates a controlled phase delay for each plane wave direction causing the wave front to converge in the focus. The image thus created is the superposition of the original plane waves minus certain high spatial frequency components. The ideal lens can thus be described by an ideal low-pass filter. Its cutoff frequency is determined by the numerical aperture NA of the lens and the wavelength λ as shown in Figure 2. due to the fact that the lens can only capture plane waves with $k_x/k_z < X/f$.

Lens aberration effects lead to an additional phase error, which renders the lens transfer function to:

$$G_{Lens} = e^{iL(k_x, k_y)}, \quad \forall \sqrt{k_x^2 + k_y^2} < \frac{2\pi NA}{\lambda}, \quad 0 \text{ otherwise} \tag{7}$$

As a result, the calculation of the field in the image plane is reduced to the calculation of the field in

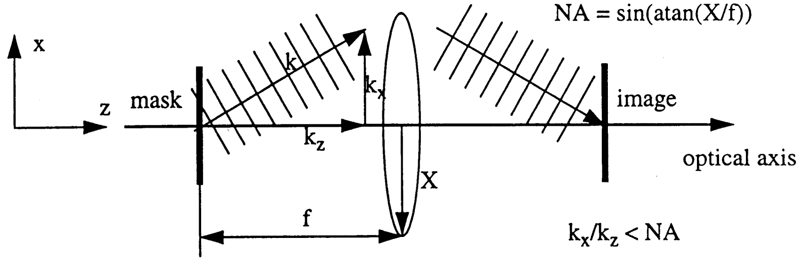

Figure 2. Derivation of the lens transfer function.

the mask plane and applying the two linear filters (6) and (7). The field in the mask plane given a single monochromatic light source is a product of a linear phase function times the mask transmittance and phase delay, which is spatially dependent for a phase-shift mask. The linear phase function is described by the complex exponential in the equation below:

$$\varphi(x, y;0) = Mask(x, y) \cdot e^{i(\alpha_x x + \alpha_y y)} \tag{8}$$

The aerial image for a single monochromatic point source is thus given by:

$$\varphi(x, y;z) = F^{-1}\{G(\Delta z) \cdot G_{Lens} \cdot F\{\varphi(x, y;0)\}\} \tag{9}$$

Fourier transforms are evaluated numerically using the Fast Fourier Transform algorithm with the number of operations given by $O(N\log N)$, with N being the total number of sampling points. An interesting and practically important aspect of evaluating eq. (9) is that while the low-pass nature of the lens transfer function ensures that the Fourier transform of the aerial image is band-limited with no spectral components for frequencies higher than $2\pi NA/\lambda$, the transform of the mask image is not band-limited. As a consequence, special care must be paid to calculating the forward transform in eq. (9) to keep aliasing errors sufficiently small.

Typical light sources in optical lithography are not coherent. To calculate the light intensity resulting from a larger light source we thus have to perform a numerical integration over the source. In other words the light source is represented by a number of point sources and the total light intensity is calculated as a weighted sum of the light intensities produced by each point source.

The total numerical effort involved is one FFT to calculate the transform of the mask image and a number of inverse transforms according to the discretization of the source. For different locations of the point source the Fourier Transform of the field in the mask plane is simply shifted by a distance in frequency domain according to the location of the point source.

3 Extraction of Printability

Calculating the aerial image numerically according to eq. (9) leaves us with a sampled image. Its sampling density is determined by the cut-off frequency $2\pi NA/\lambda$. The image can be output in a standard format (GIF) for display. Since the aerial image is band-limited, trigonometric interpolation can be used to generate additional sampling points if desired. The sampled aerial image can be directly compared to the sampled mask information to determine the quality of the aerial image. Degradation of quality is

defined as image details which are likely not to print as desired. Two cases of quality loss can be distinguished:

i) image intensity is below a threshold value in an open mask region.

ii) image intensity is above a threshold in a dark mask region.

This comparison is carried out locally for each sampling point in the image. Following [8] and others we use a value of 0.3 for both thresholds, with 1 being the aerial image intensity at the center of a large open mask region

4 Application

A test mask layout of the size 15x15 µm was chosen as an example of application. The layout is a combination of the test pattern reported in [7] and some additional mask features. Figure 3. (left) shows the aerial image calculated for λ=0.365µm, NA=0.55, Δz=0.4µm and a single centered point light source. The line thickness is 0.35 µm, which is very close to the theoretical resolution limit of $0.5 \cdot \lambda/NA \approx 0.33\mu m$. As a consequence, loss of resolution is clearly visible. Figure 3. (right) displays the results of a printability analysis, where mask areas which are likely not to print as desired are marked in gray.

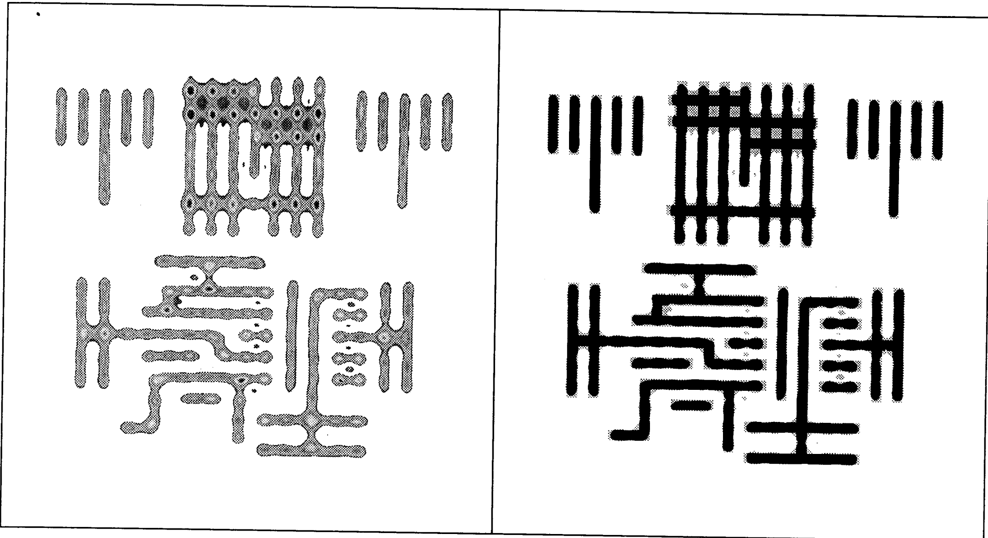

Figure 3. Application example: Aerial image and Printability analysis of a test mask pattern.

The author acknowledges helpful discussions on the subject of optical lithography with Dr. D. Bernard of TMA.

References

[1] O.W. Otto, J.G. Garofalo, K.K. Low, C.-M. Yuan, R.C. Henderson, C. Pierrat, R.L. Kostellak, S. Vaidya, P.K. Vasudev, "Automated Optical Proximity Correction - A Rules-Based Approach", *SPIE* Vol. 2197, 1994

[2] Technology Modeling Associates, DEPICT User Manual, 1994

[3] UC Berkeley, SPLAT

[4] H. Fleischer and V. Axelrad, "Fourier-Acoustics: An Approach to Acoustic Field Analysis", *Acustica*, vol. 57, 1985

[5] H. Fleischer and V. Axelrad, "Restoring an Acoustic Source from Pressure Data Using Wiener Filtering", *Acustica*, vol. 60, 1986

[6] C. Spence, J. Nistler, E. Barouch, U. Hollerbach and S. Orszag, "Automated Determination of CAD Layout Failures Through Focus: Experiment and Simulation", *SPIE* Vol. 2197, 1994

[7] N. Shiraishi, S. Hirukawa, Y. Takeuchi and N. Magome, Proc. *SPIE* 1674, p. 741, 1992

[8] D.C. Cole, E. Barouch, U. Hollerbach, S.A. Orszag, "Derivation and Simulation of Higher Numerical Aperture Scalar Aerial Images", *Jpn. J. Appl. Phys.*, Vol. 31, Pt. 1, No. 12B, 1992